Targeted Killing of Cancer Cells *in Vivo* and *in Vitro* with EGF-Directed Carbon Nanotube-Based Drug Delivery

Ashwin A. Bhirde,[†] Vyomesh Patel,[§,*] Julie Gavard,[§] Guofeng Zhang,[⊥] Alioscka A. Sousa,[⊥] Andrius Masedunskas,[§] Richard D. Leapman,[⊥] Roberto Weigert,[§] J. Silvio Gutkind,[§,*] and James F. Rusling[†,‡,*]

[†]Department of Chemistry, University of Connecticut, Storrs, Connecticut 06269, [‡]Department of Cell Biology, University of Connecticut Health Center, Farmington, Connecticut 06032, [§]Oral and Pharyngeal Cancer Branch, National Institute of Dental and Craniofacial Research, National Institutes of Health, Bethesda, Maryland 20892, and [⊥]Laboratory of Bioengineering and Physical Science, National Institute of Biomedical Imaging and Bioengineering, National Institutes of Health, Bethesda, Maryland 20982

ABSTRACT Carbon nanotube-based drug delivery holds great promise for cancer therapy. Herein we report the first targeted, *in vivo* killing of cancer cells using a drug-single wall carbon nanotube (SWNT) bioconjugate, and demonstrate efficacy superior to nontargeted bioconjugates. First line anticancer agent cisplatin and epidermal growth factor (EGF) were attached to SWNTs to specifically target squamous cancer, and the nontargeted control was SWNT-cisplatin without EGF. Initial *in vitro* imaging studies with head and neck squamous carcinoma cells (HNSCC) overexpressing EGF receptors (EGFR) using Qdot luminescence and confocal microscopy showed that SWNT-Qdot-EGF bioconjugates internalized rapidly into the cancer cells. Limited uptake occurred for control cells without EGF, and uptake was blocked by siRNA knockdown of EGFR in cancer cells, revealing the importance of EGF-EGFR binding. Three color, two-photon intravital video imaging *in vivo* showed that SWNT-Qdot-EGF injected into live mice was selectively taken up by HNSCC tumors, but SWNT-Qdot controls with no EGF were cleared from the tumor region in <20 min. HNSCC cells treated with SWNT—cisplatin—EGF were also killed selectively, while control systems that did not feature EGF-EGFR binding did not influence cell proliferation. Most significantly, regression of tumor growth was rapid in mice treated with targeted SWNT—cisplatin—EGF relative to nontargeted SWNT-cisplatin.

KEYWORDS: oral cancer · nanomedicine · intravital two-photon microscopy · carbon nanotubes · EGFR · EGF · quantum dots · cisplatin

Advanced drug delivery systems (DDS) hold great promise for improving cancer therapy outcomes.[1] Anticancer DDS based on liposomes and/or polymers were approved recently for clinical use, already favorably impact cancer treatments, and cost about the same as free drugs.[2] Ligand- or antibody-directed delivery of drugs to tumors by binding to cancer cell surface receptors or antigens has found success in current DDS.[3] Nevertheless, future challenges remain, including improving specificity and stability, regulating bioavailability, and developing lower toxicity carriers.[3−5] Head and neck squamous cell carcinoma (HNSCC) is one of the most common types of cancer in oral oncology, representing ~6% of all cases and accounting for an estimated 650000 new cancers and ~350000 cancer deaths globally per year.[6,7] Selectively targeting of squamous tumors is a long standing problem, since the drugs used lack specificity and cause severe side effects.[8,9] Thus, developing new, effective tumor-targeted drug delivery systems is of high value.

Single-wall carbon nanotubes (SWNT) present remarkable opportunities to meet future DDS challenges.[10−12] Facile strategies are available to link biological molecules like proteins, DNA, and smaller molecules onto SWNTs.[13−15] The resulting solubilized nanotubes readily enter cells by endocytosis and by other mechanisms.[16,17] Functionalized, solubilized SWNTs can transport peptides, proteins, genes, and DNA[18−22] across cell membranes with little cytotoxicity.[23,24] SWNTs also provide very high surface area per unit weight for high drug loading. Carbon nanotubes and nanohorns have been tested *in vitro* for delivery of drugs.[25−28] However, assessing the *in vivo* efficacy of nanotubes loaded with anticancer drugs is critical. Several previous reports have demonstrated *in vivo* targeting of tumors with carbon nanotubes in animal models, but with no drug cargo delivered.[29,30] While the present paper was in preparation, a report appeared describing *nontargeted* delivery of paclitaxel on SWNTs in mice.[31]

Herein, we provide the first demonstration that *targeted* SWNT drug delivery results in rapid decrease of tumor size in mice compared to a nontargeted SWNT control. SWNTs were functionalized with first-line anticancer drug cisplatin[32,33] and epidermal

*Address correspondence to james.rusling@uconn.edu, gutkind@dir.nidcr.nih.gov, vpatel@dir.nidcr.nih.gov.

Received for review September 2, 2008 and accepted December 30, 2008.

Published online January 13, 2009. 10.1021/nn800551s CCC: $40.75

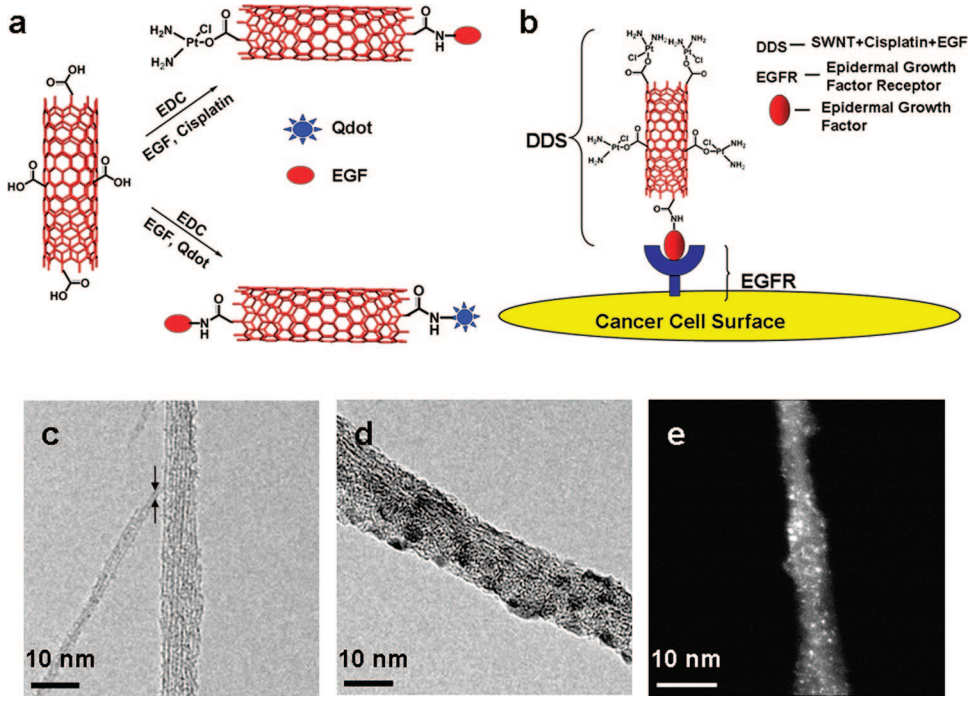

Figure 1. Nanotube-based delivery system. (A) Illustration of chemical reactions used to attach EGF, cisplatin, and Qdots onto carboxylated SWNTs (in red) using EDC as the coupling agent. (B) Schematic showing SWNT bundles bioconjugated with EGF and cisplatin targeting the cell surface receptor EGFR on a single HNSCC cell. Transmission electron micrographs of (c) oxidized SWNT bundles with arrows showing a single SWNT, (d) SWNT-Qdot-EGF bioconjugate bundle, (e) STEM image of SWNT bundle showing cisplatin as the bright spots. (scale bar = 10 nm)

growth factor (EGF) to make a DDS that selectively targets squamous cancer cells (Figure 1a,b). This new DDS capitalizes on the specific affinity of EGF for its cognate cell-surface receptor (EGFR), overexpressed in most squamous cancer cells,[34−36] as a guidance mechanisms to deliver therapeutic drug to the tumor. The present study demonstrates first that drug-laden SWNTs can selectively enter and kill cancer cells *in vitro* by utilizing EGF-EGFR interactions, and then demonstrates efficacy in an animal model.

RESULTS

Preparation and Characterization of SWNT Bioconjugates. SWNTs were oxidized in acid to provide carboxylate groups on ends and sidewalls.[10,12] These shortened nanotubes were used to prepare SWNT−cisplatin−EGF bioconjugates for cell killing, and SWNT-Qdot-EGF (Figure 1a) to visualize[37] the bioconjugates in cell cultures and mice. Uptake of the bioconjugates into target cells was visualized by luminescence of green emitting Qdot525 and red emitting Qdot605, Qdots and EGF were attached by amidization to the carboxylated SWNTs using aqueous 1-(3-(dimethylamino)propyl)-3-ethylcarbodiimide hydrochloride (EDC) as promoter.

The resulting bioconjugates were characterized by transmission electron microscopy (TEM). When coupling agent EDC was omitted from bioconjugation reactions, nanotube-like images appeared striated, with widths suggesting small bundles of 5 to 8 of individual 1.0 to 1.4 nm diameter SWNTs, but with no particles attached (Figure 1c). In contrast, with EDC in the bioconjugation mixture, decoration of nanotubes with visible small particles attached was observed (Figure 1d). The QDots are ~4 nm in average diameter, roughly corresponding to the diameters of spherical features attached to the nanotube bundles in Figure 1d. Average nanotube dimensions with dispersions were estimated from TEM as 110 ± 50 nm length and 10 ± 3 nm width.

EGF attachment was confirmed by using fluorescein-labeled EGF to make EGF−SWNT bioconjugates with increased luminescence compared to controls with no label. Luminescence was also observed from fluorescein-labeled antibodies to EGF when bound to EGF−SWNT further confirming EGF attachment (Supporting Information, Figure S1). Difference absorption spectroscopy was used to measure 3 mg mL^{-1} EGF per 1 mg mL^{-1} SWNT in dispersions, which translates to an average of 36 ± 10 EGF molecules per 100 nm length of SWNT. Cisplatin [$Cl_2Pt(NH_2)_2$] was attached *via* complexation with the nanotube carboxylate group, a ligand exchange reaction reported previously for carboxylic acids (RCOOH) attached to peptides that gave R-COO-$PtCl(NH_2)_2$ and (R-COO-)$_2PtCl(NH_2)_2$ complexes active against cancer.[38] The amount of cisplatin measured by difference UV absorbance of adsorbate solutions before and after attachment to SWNTs. Cisplatin was also detected by scanning transmission electron microscopy and energy-dispersive X-ray analysis (EDAX)[39] (Figure 1e) (Supporting Information, Figure S2). The final SWNT−cisplatin−EGF dispersions used below contained 1.3 μM cisplatin and 0.25 mg mL^{-1} SWNTs. All bioconjugates were used within several days of preparation.

Selective Targeting of HNSCC Cells with SWNT Bioconjugates *in Vitro*. We next explored whether SWNT functionalized with EGF targets EGFR on HNSCC cultures *in vitro* (Figure 1b). Representative HNSCC cell lines (HN12, HN13; see Supporting Information for cell culture conditions) previously shown to overexpress EGFR[40] were incubated for 10 min with freshly prepared SWNT−Qdot525−EGF (SQE) bioconjugates. The

location of SWNT−Qdot−EGF in HN13 cells was shown by green fluorescence of Qdot525 (Figure 2a−c) using confocal microscopy. Here, nuclei are shown in red, along with actin in blue-labeled submembrane areas. The green fluorescence observed in close proximity to the nuclei indicates intracellular accumulation of SWNT−Qdot525−EGF. The 3D reconstruction of confocal z sections (Figure 2d−f) shows SWNT−Qdot525−EGF incorporated inside the cells, bordered by the blue actin labels, confirming the translocation of SWNT−Qdot525−EGF through the cell membrane.

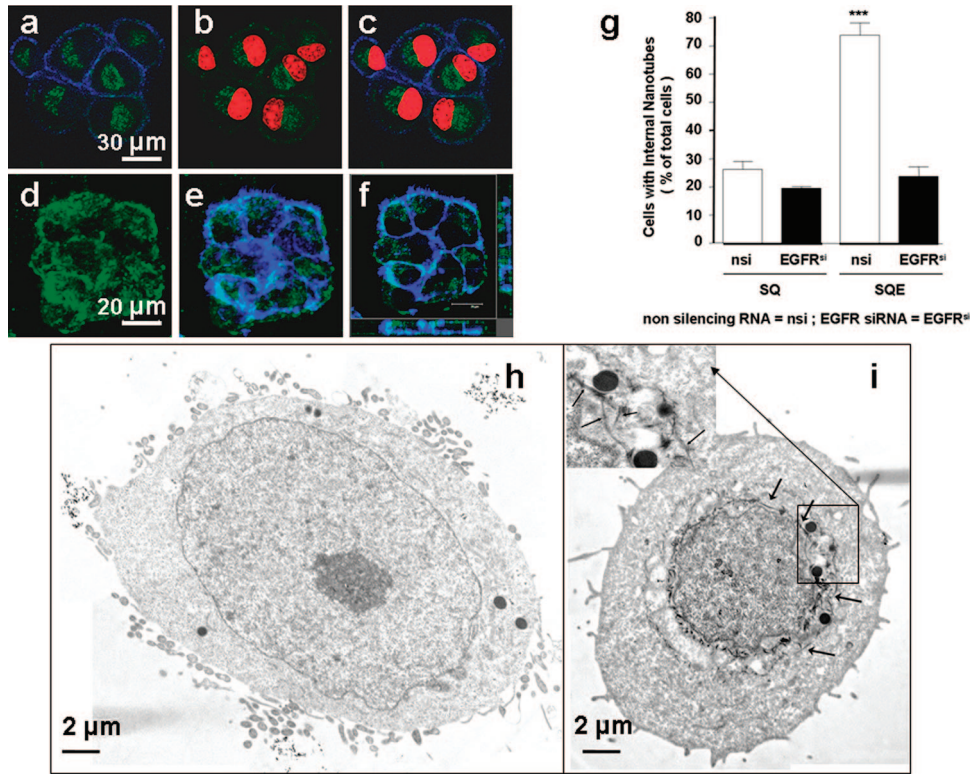

Figure 2. Cellular internalization and selective uptake of SWNT−Qdot525−EGF by HN13 cells. (a−c) *z*-Section micrographs of interiors of cells treated with SWNT−Qdot525−EGF (SQE) bioconjugates and analyzed by confocal microscopy: (a) images show the fluorescence of SQE (green) inside the cells and within the outer boundary limits of membrane as judged by actin stained by phalloidin (blue); (b) nuclei are illuminated with propidium iodide (red), and Qdots are seen in close proximity (green); (c) overlay of panels a and b showing internalization of SQE around the perinuclear region. (Scale bar = 30 μm). 3D reconstitutions of confocal *z*-sections recapitulate the localization of Qdots (green) and within the periphery of actin fibers (blue) proximal to the cell membrane. (d, e) *z*-Stacked images showing (d) nanotube-Qdot color only; (e) with nanotube-Qdot and cell membrane colors; (f) three-dimensional reconstruction of panel e in *xyz* format. On the right is shown the *z*-stack going upward from the *x* axis; on the bottom is shown the *z*-stack going upward from the *y* axis. Scale bars = 20 μm. (g) Quantification of results here and in Supporting Information, Figure S4 demonstrates that when the bioconjugate includes EGF and the cells retain high EGFR expression levels, the cells have the largest amount of bioconjugate internalization. The label EGFR^{si} means treatment with active siRNA to knockdown EGFR. *t* tests indicated significant differences between control/SQE and the other samples at $p < 0.05$ using ANOVA (***). (h, i) Cells incubated with SQ or SQE and subsequently washed and subjected to TEM: (h) cells exposed to SQ only, no features resembling internalized nanotubes detected; (i) cells treated with SQE show dark cylindrical structures resembling nanotubes (indicated by arrows) around the perinuclear region, presumably internalized bundles of SWNTs; the inset shows a higher magnification image with nanotubes indicated by arrows. Scale bars are 2 μm.

Intracellular Qdot luminescence was detected in HN13 cells only when EGF was included as a targeting ligand on the bioconjugate, suggesting the high specificity of the EGF-dependent intracellular accumulation of labeled SWNTs in cancer cells. We demonstrated that internalization of the bioconjugates is directed by EGF binding to EGFR by knocking down the receptors on HNSCC cells using siRNA.[41,42] Whereas nonsilencing RNA (nsi) did not affect EGFR expression, this receptor was nearly undetectable in cells transfected with siRNA for EGFR (EGFR^{si}, Supporting Information, Figure S3). Cells with diminished levels of EGFR showed low, basal uptake of nanotubes regardless of EGF presence, but did not specifically internalize SWNT−Qdot525−EGF (Supporting Information, Figure S4,a−d). This finding is reflected by quantitative analysis of the confocal micrographs (Figure 2g), in which the percentage of cells with internalized SWNT−Qdot525−EGF was >75% for nontransfected HN13 cells with EGFR compared to <20% for controls lacking or expressing low levels of EGFR. Analysis of pixel intensities in the micrographs also indicated a similar profile for the internalization (Supporting Information, Figure S5).

Collectively, these results suggest that EGF−EGFR ligand−receptor interactions mediate efficient internalization of SWNT−Qdot−EGF, most likely by receptor-mediated endocytosis.[16,43] A fraction of cells lacking EGFR internalized some SWNT−Qdot−EGF, suggesting a secondary mechanism possibly related to that in systems where endocytosis is not possible.[17] Internalized SWNT−Qdot525−EGF bioconjugates were also observed by TEM[44] in HN13 cells. In cells exposed to SWNT−Qdot only, SEM features resembling nanotubes were not detected (Figure 2h). In contrast, SQE-treated cells clearly showed tubular structures indicating the presence of the nanotube bioconjugates in close proximity to the perinuclear region (Figure 2i). Nanotube bioconjugates were also found distributed around lysosomes and within the cytoplasm. The nanotubes ob-

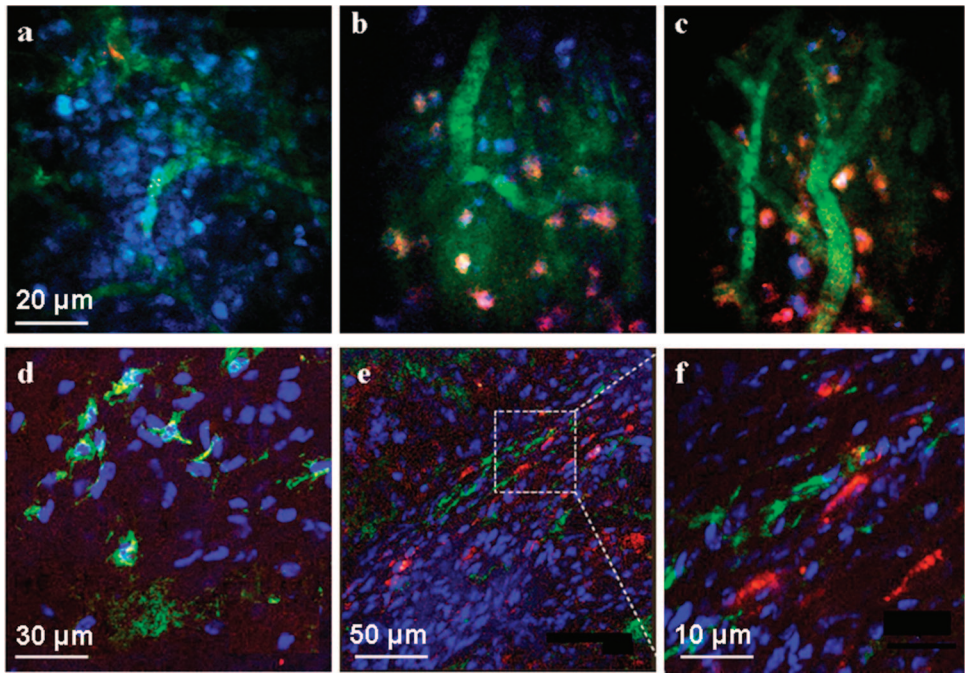

Figure 3. Detection of nanotube bioconjugates in tumors *in vivo*. Representative frames from time-lapse videos acquired by 3-color, intravital two-photon microscopy (a−c). Mice bearing the HN12 xenografts were anesthetized and treated with SQ or SQE (red) bioconjugates. Cell nuclei were stained with Höechst (blue) and blood vessels with 500 kDa FITC-dextran (green): For SQ alone with no EGF (a), very little or no red fluorescence representing the Qdot signal was detected within the tumor mass 45 min after injection. Two different views after administration of SQE giving red fluorescence 45 min post injection within the tumor microenvironment (b,c). The red SQE bioconjugate is localized in close proximity to the nuclei suggesting its internalization by the tumor cells within the xenograft. (Scale bar in a−c is 20 μm). Confocal microscopy images of fixed xenograft cryosections (d−f) In the SQ treated tumor sections (d), only Höechst stained cell nuclei (blue) and vascular FITC-labeled dextran (green) are visible (scale bar 30 μm). (e) In SQE treated mice, characteristic red fluorescence was widely distribution within the tumor microenvironment. (scale bar 50 μm). (f) Magnified dotted region of panel e showing internalized SEQ bioconjugates the cells within the tumor mass. (scale bar 10 μm).

served in TEM are most likely aggregates, since they have diameters of ~10 nm, much larger than the ~1.4 nm average diameter of single nanotubes. Lengths of tubular TEM features of 50−300 nm were similar to the 40−400 nm lengths of the oxidized nanotube starting material. Few, if any, SQ bioconjugates (without EGF) were found within the plasma membrane, implying that they were unable to reach the cell nuclei, whereas SQE bioconjugates clearly were rapidly taken up, as evidenced by their accumulation in the perinuclear region (Figure 2i, and Supporting Information, Figure S6a,b).

Two-Photon Video Imaging of Mice Bearing HNSCC Tumor Treated with SWNT Bioconjugates. We next focused on determining if the EGF-EGFR interaction would direct nanotube bioconjugates to tumors *in vivo* using the HNSCC xenograft model. HN12 cells that also express EGFR[45] were used to induce tumors in athymic mice. Once tumors had grown to approximately 7−10 mm, nuclei and vasculature were visualized by intravital 3-color imaging through systemic injection of Höechst and 500 KDa FITC-labeled dextran, respectively. SWNT−Qdot605−EGF and control SWNT−Qdot605 (no EGF) were delivered systemically (Supporting Information Figure S7 and video S8) and monitored for their relative distribution. The videos are the primary data in these studies, although in the main paper we can only display individual still frames indicating a result at one instant in time. In the videos, SWNT−Qdot605−EGF could be readily observed moving with the blood flow, diffusing out from the vasculature within ~20 min postinjection and rapidly accumulating within the tumor mass (Supporting Information videos S9 and S10, and Figure 3b,c). Control bioconjugates without the targeting ligand were also detected within the blood vessels immediately after injection. These controls were rapidly cleared and never found accumulated in the tumor cells (Supporting Information video S11, and Figure 3a).

Lesions from similarly treated mice were also analyzed by confocal microscopy. Data show that only SWNT−Qdot605−EGF bioconjugates accumulated within the tumor mass (Figure 3e,f). Control experiments in which ligand−receptor interactions were absent showed little or no uptake by the tumor cells (Figure 3d). The intravital two-photon and confocal analysis also suggest that the Qdots remained attached to the nanotube bioconjugate, as the SWNT−Qdot605 bioconjugate was internalized by the tumor cells only when the EGF was included on the SWNT−Qdot bioconjugate. This can be verified by comparing EGF-free controls (Figures 3a and d) with the full bioconjugate (Figures 3b,c,e,f). The red Qdot-nanotube control conjugate does not give a color in the tumor tissue, only the full bioconjugate in which both Qdots and EGF are attached to the nanotubes, suggesting that it arrives in the tumor region intact.

***In Vitro* Killing of HNSCC Cells Using SWNT−Cisplatin−EGF.** Figure 4a shows optical micrographs of exponentially grown HN13 cells adhered to an underlying plate. After addition of SWNT−cisplatin−EGF (SCE) to the cells and incubating for 10 min, the cells showed minor morphological changes and dark nanotube bioconjugates on their surfaces (Figure 4b). After being washed in PBS and placed in fresh media, most of the nanotubes were removed, leaving only those bound to EGFR on the

cell surfaces (Figure 4c). After an additional 7−12 h incubation, a profound change in cell morphology was observed (Figure 4d). The majority of the cells were detached and floating, indicative of cell death. Apoptosis of HN13 cells treated with SWNT−cisplatin−EGF was confirmed by the TUNEL assay (supporting Figure S12).

Selective *in Vitro* Cancer Cell Targeting of SWNT Bioconjugates with Cisplatin. To examine the receptor dependence of cell death from SWNT bioconjugates, siRNA knockdown of EGFR was done on HN13 cells, as confirmed by Western blot (supporting Figure S3). Cell proliferation was estimated through mitochondrial activity (MTT assay).[46,47] Assays were done using SWNT−cisplatin−EGF and controls (cells only, cisplatin alone, and cisplatin-SWNT) using HN13 cells and those with EGFR knockdown siRNA or control siRNA without knockdown (Figure 4e). The cisplatin concentration used was within levels detected in serum of cancer patients receiving this drug (1−10 μM). Cells treated with SWNT, cisplatin (10 μM, clinically relevant), and cisplatin−SWNT without EGF showed only very small differences in growth. However, for HN13 cells and cells pretreated with control siRNA, cell growth was hindered (~25−50%) when treated with SWNT−cisplatin−EGF (1.3 μM, SCE in Figure 4e), while cells lacking EGFR were minimally affected. All cells treated with high doses of free cisplatin (300 μM, clinically irrelevant) had greatly decreased cell growth showing the efficacy of the drug under these conditions and serving as a positive control. Cell proliferation results with SWNT−transplatin−EGF, an isomer of cisplatin (supporting Figure S13), were consistent with Figure 4B and with the lower anticancer activity of this drug. Together, these results supported the high specificity of SWNT−cisplatin−EGF bioconjugates as a receptor-guided anticancer drug delivery system.

Further studies were done with SAA cells, that is, NIH3T3 cells that overexpress EGFR, and NIH3T3 cells which express much less EGFR than HN13 cells. Western blot assays for EGFR confirmed the expected high or low levels of EGFR (supporting Figure S14). Cell proliferation data (Figure 4f) show that after incubation with SWNT−cisplatin−EGF, growth was hindered in HN13 and SAA cells which overexpress EGFR, but growth of NIH3T3 cells was largely unaffected. Nanotubes alone, 10 μM free cisplatin, SWNT−EGF and SWNT−cisplatin demonstrated negligible effects on growth in any cell lines. Cells treated with a large dose of cisplatin (300 μM) again resulted in low cell proliferation indicative of severe cytotoxicity. A key result is that SWNT−cisplatin−EGF dispersions with 1.3 μM cisplatin were more effective at cell killing than 10 μM free cisplatin.

***In Vivo* Tumor Targeting of SWNT Bioconjugates with Cisplatin.** HN12 cells that also overexpress EGFR were treated with SCE in a similar way as HN13 cells and the cell proliferation was tested using MTT assay (supporting Figure S15). These cells were then used to induce tumors

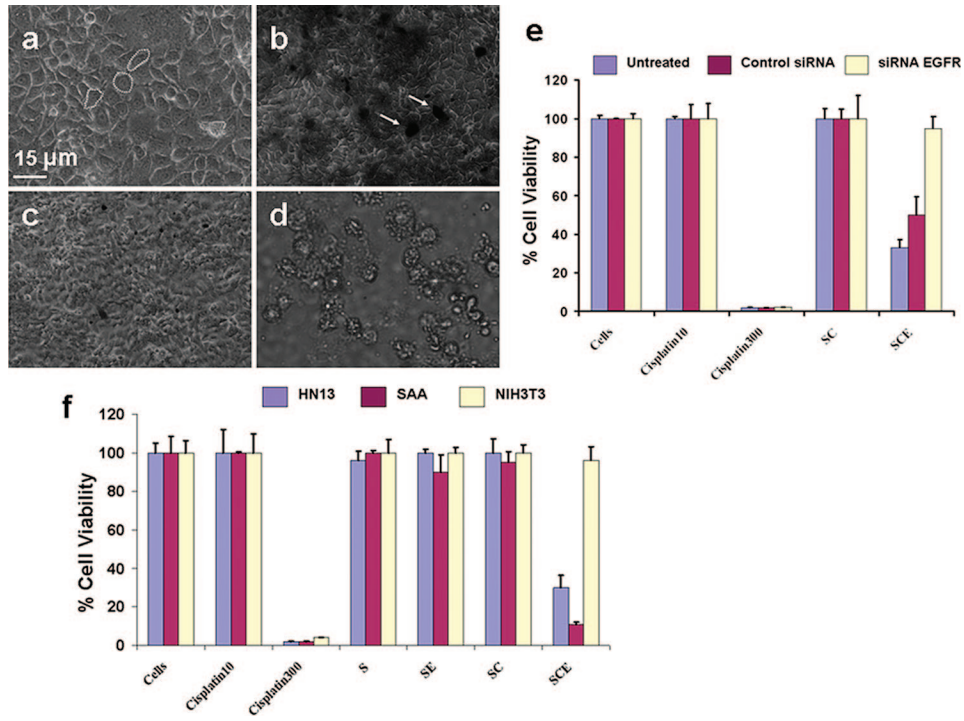

Figure 4. Selective killing of cancer cells using SWNT bioconjugates. (a−d) Optical micrographs showing targeting killing of HN13 cells with SWNT−cisplatin−EGF (SCE): (a) cells before treatment, which adhered to the plate and attached to each other with structural morphology intact; (b) cells treated with SCE for 10 min, before washing; dark regions are those with nanotubes present; (c) cells washed with PBS and resuspended in cell culture media DMEM after 10 min incubation with SEC; (d) HN13 cells (treated with SCE for 10 min and washed) after 12 h, cells appear floating detached from each other and the plate. Panels e and f are the cell viability studies. (e) Viability comparisons using cell proliferation assay after 12 h for normal HN13 cells, and HN13 cells transfected with EGFR knockdown and control (no knockdown, labeled "Untreated") siRNA: Cells, normal growth control; Cisplatin10, cells treated with 10 μM free cisplatin; Cisplatin300, incubated with 300 μM free cisplatin; SC, incubated with SWNT−cisplatin and washed with PBS after 10 min; SCE, incubated with SWNT−cisplatin−EGF (1.3 μM cisplatin) then washed with PBS after 10 min. (f) Cell viability comparisons using cell proliferation assay after 12 h for normal HN13 cells, with NIH3T3 and SAA mouse fibroblast cells: Cells, normal growth untreated; Cisplatin10, cells treated with 10 μM free cisplatin; Cisplatin300, incubated with 300 μM free cisplatin; S, incubated with SWNTs 10 min; SE, incubated with SWNT−EGF and washed with PBS after 10 min. SC, incubated with SWNT−Cisplatin and washed with PBS after 10 min; SCE, incubated with SWNT−cisplatin−EGF (1.3 μM cisplatin) then washed with PBS after 10 min.

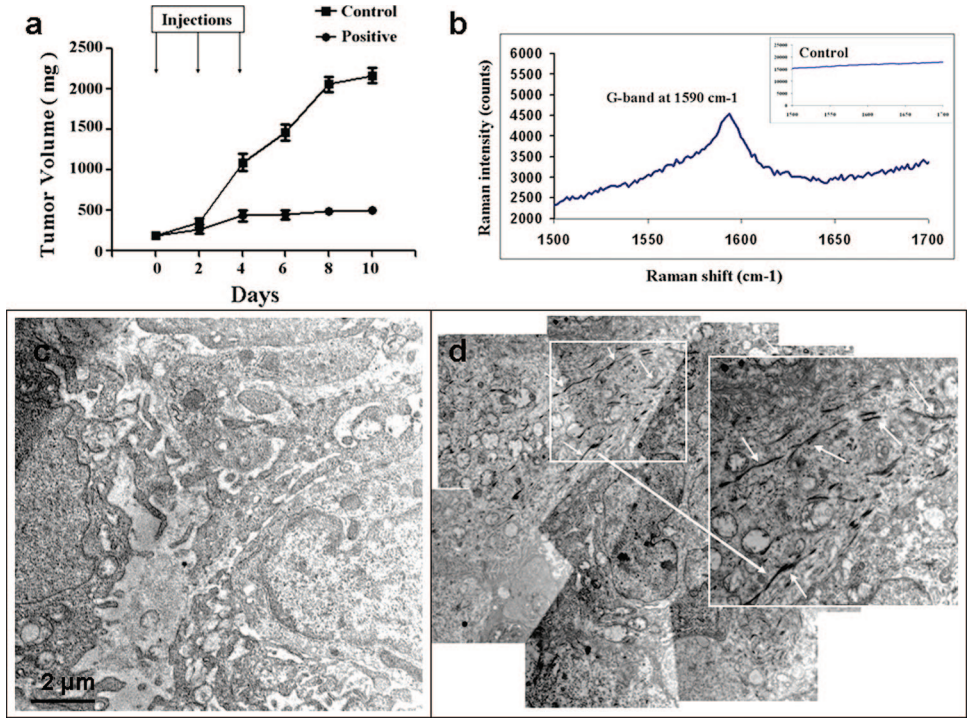

Figure 5. Inhibition of pre-established HN12 HNSCC tumor growth by SWNT−cisplatin−EGF bioconjugates. The nanotube bioconjugates injected intravenously through the tail vein and observed for the tumor progression: (a) plot showing the tumor progression with time (error bars represent S.E.M., $n = 3$); (b) Raman spectra of cryosection of positive tumor tissue; (c and d) montage of transmission electron micrograms of fixed tumor sections of mice treated with control and positive. Inset at higher magnification on the right shows the nanotubes very clearly as pointed out by the white arrows. Scale bar = 2 μm.

in nude athymic mice. Once these tumors had grown to approximately 7−10 mm, the mice were given iv injections of the nanotube bioconjugates along with the controls through the tail vein. The mice were monitored for ~2 weeks for their tumor growth pattern. Figure 5a shows tumor growth in the mice for both control (SWNT−cisplatin) and the positive bioconjugates (SWNT−cisplatin−EGF) for 10 days. The mice treated with an unguided nanotube bioconjugate (control) *did not* show tumor regression and the tumor kept on growing. Mice treated with targeted nanotube bioconjugate (positive) showed considerable slowdown in the tumor growth indicating a selective targeting of SWNT−cisplatin−EGF into the HNSCC cancer microenvironment. Raman characterization was done on tumor cryosections to detect the SWNTs. Figure 5b shows the signature G-band of SWNT obtained from a positive mouse,[48] while the Raman peaks were not detected in the control mice (supporting Figure S16). Figure 5c,d shows the TEM tumor tissue crossections from sacrificed animals after ~2 weeks treatment. The control micrographs did not show any structures resembling nanotubes while the positive electron micrograph shows very clear nanotube-like structures (200−500 nm length) suggesting the presence of the nanotube bioconjugates within the tumor. The precise mechanism through which the drug bound to the nanotubes is released and kills tumor cells is under further investigation. For example, one report suggests that cisplatin is released from poly(L-glutamic acid)−cisplatin by slow ligand exchange between chloride ions and COOH.[49]

Biodistribution in Mice. We analyzed vital organs and tumors from mice injected with the nanotube bioconjugates to monitor the short-term biodistribution of SWNT bioconjugates. Analysis of these images suggested that the SWNT-Qdot605-EGF bioconjugates are much more abundant within the microenvironment of the tumor in comparison to controls at 45 min postinjection (Figure 6). Quantitative analysis of image intensities indicated a significantly larger uptake of nanotube bioconjugates within the tumor section when the targeting ligand EGF was incorporated into the bioconjugates (supporting Figure S17). Smaller amounts of nanotube bioconjugates were found within the spleen, lung, liver, kidney and heart, as shown by the red Qdot color, and this occurred regardless of the presence of EGF. The biodistribution profile of our nanotube bioconjugates showed accumulation in different vital organs as also reported for nanotubes solubilized with PEG.[23,29]

DISCUSSION

Results above clearly demonstrate for the first time that SWNTs bioconjugated with a targeting ligand and cisplatin is superior to untargeted drug-SWNT bioconjugates for selective cancer chemotherapy in living animals (Figures 3 and 5a). Administration of the SWNT−cisplatin−EGF bioconjugate caused a very significant tumor volume decrease compared to SWNT-cisplatin control, albeit with limited numbers of mice (Figure 5). Furthermore, *in vitro* imaging (Figure 2), cell viability (Figure 4), and *in vivo* video imaging (Figure 3 and videos in Supporting Information) studies are consistent with efficient entry of EGFR-targeted nanotube bioconjugates into cancer cells, but much less efficient entry of the nontargeted controls into cells. TEM images are strongly supportive of this view, showing clear evidence of carbon nanotubes within *in vitro* cells (Figure 2) and tumor tissue sections of mice (Figure 5c,d) that had been treated with EGFR-targeted nanotubes, but little

evidence for nontargeted nanotubes in the cells in control experiments. In the mouse tissue sections, the identity of the dark cylindrical images as nanotubes was confirmed with Raman spectroscopy (Figure 5b).

Short-term biodistribution studies of these SWNT bioconjugates showed the presence of nanotube bioconjugates in various vital organs of the mice, but in much smaller amounts than in the tumors (Figure 6). Clearly, long and short-term toxicity of these and other nanotube-drug bioconjugates must be fully characterized prior to successful translation to the clinic. While needle-like multiwall CNTs $>$ 20 μm show serious toxic effects in animals,[50] shortened nanotubes (*e.g.*, $<$1 mm) functionalized with biomolecules or chemical groups to provide good aqueous solubility or dispersability show negligible cytotoxicity even at high concentrations.[51−54] On the basis of these and related studies, more efficient solubilization of nanotube bioconjugates may aid their rapid clearance and minimize toxic effects. The precise assessment of biodistribution of nanotube bioconjugates as well as their long-term cytotoxicity[55] *in vivo* is currently under further evaluation in our laboratories.

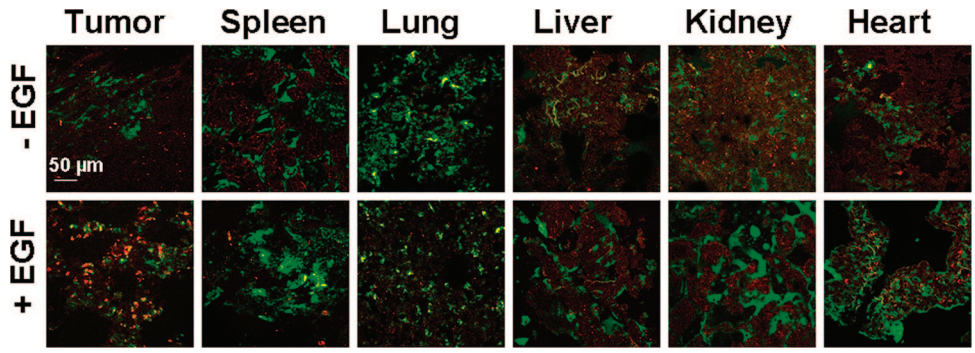

Figure 6. Analysis of the distribution of nanotube bioconjugates *in vivo*. Vital organs from tumor-bearing mice injected with Höechst, FITC-dextran, then treated with either SQ or SQE, were removed, frozen, cryosectioned, fixed, and processed for confocal microscopy. Tumor tissues indicate increased uptake of bioconjugates, shown in red, only when EGF was on the nanotubes. Spleen, liver, kidney and heart show some red fluorescence characteristic of the SWNT−Qdots irrespective of the presence or absence of EGF. The pixel intensities were further analyzed for relative quantification of SQ or SQE levels within the different tissues (see supporting Figure S17). Scale bar is 50 μm.

In vitro and *in vivo* studies herein provide clues to the mechanism of targeting and internalization of the targeted nanotube DDS into cancer cells. Internalization of the EGFR targeted SWNT-EGF bioconjugates by HNSCC cells was very fast and selective (Figure 2). Two-photon intravital videos, the primary data for the *in vivo* imaging, played a key role in tracking the fate of nanotube bioconjugates in living species, and provided direct *in vivo* evidence of targeted SWNT−Qdot−EGF bioconjugates being rapidly internalized into cancer tumors. The videos clearly show that within 20 min of administration the SWNT−Qdot−EGF bioconjugates accumulated within the periphery of the cell nuclei (Figure 3). On the contrary, the nontargeted SWNT−Qdot−EGF bioconjugates were visualized entering the vasculature but being rapidly cleared from the tumor region during a similar 20 min period. This is best visualized by viewing the time lapse videos themselves (Supporting Information videos, S8−S11), as Figure 3 shows only the images at specific points in time. Complementing these *in vivo* studies suggesting the effectiveness of targeting with EGF, *in vitro* cell proliferation assays showed definitively that ligand−receptor (EGF-EGFR) interactions are key to the targeting and killing of the cancer cells (Figure 4).

CONCLUSION

This paper presents direct evidence that oxidized SWNTs bioconjugated with cisplatin and specific receptor ligand EGF can selectively and efficiently target squamous cancer cells that overexpress EGFR as demonstrated by *in vivo* and *in vitro* imaging and cancer cell viability. EGFR-targeted bioconjugates were much more efficient at killing cancer cells than untargeted controls containing the same drug. Moreover, results suggest a major ligand receptor-mediated endocytosis pathway for cellular uptake both *in vitro* and *in vivo*, as suggested previously from *in vitro* studies,[16,18] accompanied by a less specific, less efficient secondary cell-internalization mechanism. While short-term biodistribution results of the tumor targeting SWNT DDS are promising (Figure 6), forward translation of targeted nanotube DDS will require long-term toxicity, distribution, and clearance studies in animal models. Nevertheless, findings herein strongly suggest the feasibility of future applications of SWNT bioconjugates in cancer-targeted drug delivery.

METHODS

Bioconjugation of Cisplatin, EGF, and Qdots to SWNTs. SWNTs were HiPco nanotubes from Carbon Nanotechnologies, Inc. Human epidermal growth factor (EGF), fluorescein and 1-(3-(dimethylamino)propyl)-3-ethylcarbodiimide hydrochloride (EDC) from Sigma-Aldrich was dissolved in PBS immediately before use. Amino (PEG) quantum dot nanocrystals (Qdot; 525 nM) were from Invitrogen. Cisplatin [cis-diammineplatinum(II) dichloride] was from the Development Therapeutics Program (National Cancer Institute), and *trans*-platinum(II)diammine dichloride was purchased from Sigma-Aldrich.

Shortened, oxidized SWNTs (0.5 mg/ml) were dispersed in PBS by sonication for 5 min followed by incubation with 2 mg/mL EDC for 1 min at room temperature (RT), after which samples were immediately vortexed. Next EGF was added to-

gether with either cisplatin (10 μM in DMSO) or Qdots (8 μM solution), and the resulting mixture reacted for an additional 1 h at 37 °C in a thermomixer. These samples were then centrifuged at 1300 rpm for 20 min and the resulting SWNT−cisplatin−EGF (SCE) or SWNT−Qdot−EGF (SQE) were resuspended in 100 μL DMEM and used immediately. Control SCE and SQE (minus EGF or cisplatin or Qdot), and bioconjugates where cisplatin was replaced with *trans*-platinum(II)diammine dichloride were prepared similarly.

Cell Proliferation (MTT) Assay. Cells were grown to 50−60% confluency overnight in 96 well plates. Next, the media was aspirated and the cells incubated with fresh media containing SCE and control complexes for 10 min. After 3 washes in PBS, cells were incubated for an additional 24 h in fresh media. MTT was assessed using the CellTiter 96 AQ One Solution Cell Proliferation Assay kit (Promega, MI), and measured optically at 570 nm.

Animal Studies. All animal studies were carried out according to NIH-approved protocols, in compliance with the Guide for the Care and Use of Laboratory Animals. Female athymic (*nu/nu*) nude mice (Harlan Sprague−Dawley, Indianapolis, IN), 4−6 weeks old and weighing 18 to 20 g were used in the study, housed in appropriate sterile filter-capped cages, and fed and given water ad libitum. HN12 cells maintained as described (see above) were transplanted subcutaneously into the flanks of mice to induce HNSCC tumor xenografts as previously described.[46]

Biodistribution Studies. Animals with xenografts of approximately 7−10 mm in length were injected intravenously (iv) with Höechst (3342) and FITC (fluorescein isothiocyanate)-dextran (500 kDa) stains (Invitrogen) followed by SWNT−Qdot605−EGF or SWNT−Qdot605 (0.6 mg in 200 μL PBS) bioconjugates. After euthanasia (~1 h post injection), vital organs (heart, kidney, liver, lung, spleen) and tumors were removed from the animals, and part fixed and paraffin embedded, or frozen and embedded in optimal cutting temperature compound Tissue-Tek OCT (Sakura Finetek USA, Inc., Torrance, CA). For *in vivo* biodistribution studies, color channel from each of the confocal images (see above) was acquired using a triple filter set as high-resolution TIFF images (Figure 5).

Confocal Microscopy. HN13 and corresponding siRNA transfected cells were grown 50−60% confluent on glass coverslips, treated with SWNT−Qdot−EGF and SWNT−Qdot bioconjugates as described above and, incubated for an additional 1 h post-treatment. Cells were next fixed in 3.5% PBS-formaldehyde solution for 15 min at RT, followed by rinses in PBS (3 × for 2 min each), permeabilization in 0.5% PBS-Triton X100 solution for 5 min at RT, after which the cells were blocked with 3% PBS−BSA solution for 30 min at RT. Cells were next incubated with AlexaFluor 647-conjugated phalloidin (1/500 dilution in PBS for 45 min at RT; Invitrogen). Nuclei were revealed using propidium iodide (1/10000 dilution in H_2O for 5 min at RT; Invitrogen). After 5× washing, samples were mounted onto SuperFrost microslides with Vectashield mounting medium (Vector Laboratories, Inc., Burlingame, CA). Eight micrometer cryosections of xenografts retrieved from mice that had been injected intravenously with SWNT−Qdot−EGF and SWNT−Qdot bioconjugates were prepared, fixed (in 90% ethanol for ~30 s) mounted and analyzed directly under confocal microscope without any additional staining. In all cases, confocal acquisitions were performed with a TCS/SP2 Leica microscope and pictures are representative of at least three independent experiments. Images were processed and analyzed using Metamorph Premier 7.1 software (Molecular Devices, Sunnyvale, CA). Statistical analyses were conducted with Prism 4.0 software (GraphPad Inc. San Diego, CA).

Transmission Electron Microscope Imaging. Electron microscope imaging was done using FEI CM120 transmission electron microscope (TEM; equipped with a Gatan GIF100 image filter) operating at a beam energy of 120 keV for *in vitro* and *in vivo* studies of SWNT bioconjugates and Tecnai TF30 TEM (FEI, Hillsboro, OR) equipped with a Gatan Ultrascan 1000 CCD camera (Gatan, Pleasaton, CA) for characterization of SWNT bioconjugates. EDX analysis for Pt was done using a VG HB501 dedicated scanning transmission electron microscope operating at 100 kV and equipped with an Oxford energy-dispersive X-ray microanalysis system.[56] (Full details in Supporting Information file.)

Two-Photon Intravital Video Microscopy. Time-lapse acquisitions were performed using an Olympus IX81 microscope (Olympus, Melville, NY) customized for two-photon microscopy. Fluorescent probes were excited with an infrared beam (800 nm) generated by a tunable Ti:Sapphire femtosecond laser, Chameleon Ultra II (Coherent, Santa Clara, CA). The power was modulated using a combination of neutral density filters (Chroma Technologies, Rockingham, VT) and maintained at the specimen between 10−30 mW. The diameter of the beam was modulated using a beam expander (LSM Technology Inc., Shrewsbury, PA) and directed into a Fluoview 1000 scanning head (Olympus, Melville, NY). The beam was focused on the specimen *via* a water immersion objective (UPLSAPO 60X NA 1.2; Olympus America Inc.) mounted on an objective inverter (LSM technologies, Stewartstown PA). A carbomer 940-based gel (Snowdrift farm, Tucson, AZ) was used as optical coupling media. The emitted light was gathered through the same objective and directed into a custom-made array of three nondescanned detectors that were installed on the right port of the microscope (LSM Technology Inc., Shrewsbury, PA). Three cooled PMTs (R6060−12, Hamamatsu Photonics K.K, Hamamatsu, Shizuoka Prefecture, Japan) were used to detect the spectrally separated emitted light. Höechst fluorescent signal was detected on the first PMT (dichroic mirror, 510 nm; barrier filter, 400−480 nm). FITC was detected on the second PMT (dichroic mirror, 570 nm; barrier filter, 505−560 nm) and Qdot605 on the third PMT (barrier filter, 590−650 nm). The animals were anesthetized by an intraperitoneal injection of a mixture of ketamine and xylazine 125 and 25 mg/kg body weight, respectively. The anesthetized animals were placed on an adjustable stage on the side of the microscope. The stage was preheated to protect animals from hypothermia. For the systemic injections, the tail artery was surgically exposed, and a small incision was performed to insert a fine catheter connected to a 1 mL syringe filled with saline (supporting Figure S7). The nuclei were stained by systemic injection of 2.5 μg of Höechst (3342) and the blood volume was labeled by injection of 20 μg of FITC-Dextran (500 kDa). Both probes were purchased from Invitrogen and dissolved in saline. Approximately 0.06 mg of SWNT−Qdot605-EGF and SWNT−Qdot605 (control) bioconjugate suspended in 200 μL PBS was injected systemically. Time-lapse acquisition was started just prior to injecting the bioconjugates and continued for up to 1 h. Acquisitions speed was set 0.3 frames per second. Videos were assembled with Metamorph (Molecular Devices, Sunnyvale, CA) and compressed with QuickTime Pro.

Acknowledgment. This research was supported by the intramural programs of the National Institute of Dental and Craniofacial Research and the National Institute of Biomedical Imaging and Bioengineering, NIH, and in part by PHS grant ES013557 from NIEHS/NIH.

Supporting Information Available: Materials and methods for SWNT bioconjugation, cell culture, Western blot, animal studies, confocal microscopy, TEM, Raman, bright field optical microscope imaging, and *in vivo* two-photon fluorescence microscopy videos. This material is available free of charge *via* the Internet at http://pubs.acs.org.

REFERENCES AND NOTES

1. Ferrari, M. Cancer Nanotechnology: Opportunities and Challenges. *Nat. Rev. Cancer* **2005**, *5*, 161–171.
2. Moses, M.; Brem, H.; Langer, R. Advancing the Field of Drug Delivery: Taking Aim at Cancer. *Cancer Cell* **2003**, *4*, 337–341.
3. Singha, R.; Kim, G. J.; Nie, S.; Shin, D. M. Nanotechnology in Cancer Therapeutics: Bioconjugated Nanoparticles for Drug Delivery. *Mol. Cancer Ther.* **2006**, *5*, 1909–1917.
4. Allen, T.; Cullis, P. Drug Delivery Systems: Entering the Mainstream. *Science* **2004**, *303*, 1818–1822.
5. Moghimi, S. M.; Hunter, A. C.; Murray, J. C. Long-Circulating and Target-Specific Nanoparticles: Theory to Practice. *Pharmacol Rev.* **2001**, *53*, 283–318.
6. Aigiris, A.; Karamouzis, M.; Raben, D.; Ferris, R. Head and Neck Cancer. *Lancet* **2008**, *371*, 1695–1709.

7. Jaracz, S.; Chen, J.; Kuznetsova, L. V.; Ojima, I. Recent Advances in Tumor-Targeting Anticancer Drug Conjugates. *Bioorg. Med. Chem.* **2005**, *13*, 5043–5054.
8. Vreeburg, G.; Stell, P.; Holding, J.; Lindup, W. Cisplatin-Albumin Complex for Treatment of Cancer of the Head and Neck. *J. Laryngol. Otol.* **1992**, *106*, 832–833.
9. Jongh, F.; Veen, R.; Veltman, S.; Wit, R.; Burg, M.; Bent, M.; Planting, A.; Graveland, W.; Stoter, G.; Verweij, J. Weekly High-Dose Cisplatin is a Feasible Treatment Option: Analysis on Prognostic Factors for Toxicity in 400 Patients. *Br. J. Cancer* **2003**, *88*, 1199–1206.
10. Dai, H. Carbon Nanotubes: Synthesis, Integration and Properties. *Acc. Chem. Res.* **2002**, *35*, 1035–1044.
11. Bianco, A.; Kostarelos, K.; Prato, M. Opportunities and Challenges of Carbon-Based Nanomaterials for Cancer Therapy. *Expert Opin. Drug Delivery* **2008**, *5*, 331–342.
12. Dresselhaus, M. S.; Dresselhaus, G.; Avouris, P., Eds. Carbon Nanotubes: Synthesis, Structure, Properties, and Applications. *Topics in Applied Physics*; Springer: Berlin, 2001; Vol. 80.
13. Bianco, A.; Kastarelos, K.; Partidos, C.; Prato, M. Biomedical Applications of Functionalised Carbon Nanotubes. *Chem. Commun.* **2005**, 571–577.
14. Chen, R. J.; Bangsaruntip, S.; Drouvalakis, K. A.; Kam, N. W. S.; Shim, M.; Li, Y.; Kim, W.; Utz, P. J.; Dai, H. Noncovalent Functionalization of Carbon Nanotubes for Highly Specific Electronic Biosensors. *Proc. Nat. Acad. Sci. U.S.A.* **2003**, *100*, 4984–4989.
15. Singh, R.; Pantarotto, D.; McCarthy, D.; Chaloin, O.; Hoebeke, J.; Partidos, C.; Briand, J.; Prato, M.; Bianco, A.; Kostarelos, K. Binding and Condensation of Plasmid DNA onto Functionalized Carbon Nanotubes: Toward the Construction of Nanotube-based Gene Delivery Vectors. *J. Am. Chem. Soc.* **2005**, *127*, 4388–4396.
16. Kam, N. W.; Liu, Z.; Dai, H. Carbon Nanotubes as Intracellular Transporters for Proteins and DNA: An Investigation of the Uptake Mechanism and Pathway. *Angew. Chem., Int. Ed.* **2006**, *45*, 577–581.
17. Kostarelos, K.; Lacerda, L.; Pastorin, G.; Wu, W.; Wieckowski, S. B.; Luangsivilay, J.; Godefroy, S.; Pantarotto, D.; Briand, J.-P.; Muller, S.; Prato, M.; Bianco, A. Cellular Uptake of Functionalized Carbon Nanotubes is Independent of Functional Group and Cell Type. *Nat. Nanotechnol.* **2007**, *2*, 108–113.
18. Kam, N. W. S.; Dai, H. Carbon Nanotubes as Intracellular Protein Transporters. Generality and Biological Functionality. *J. Am. Chem. Soc.* **2005**, *127*, 6021–6026.
19. Pantarotto, D.; Briand, J.; Prato, M.; Bianco, A. Translocation of Bioactive Peptides Across Cell Membranes by Carbon Nanotubes. *Chem. Commun.* **2004**, 16–17.
20. Liu, Y.; Wu, D.; Zhang, W.; Jiang, X.; He, C.; Chung, T.; Goh, S.; Leong, K. Polyethylenimine-Grafted Multiwalled Carbon Nanotubes for Secure Noncovalent Immobilization and Efficient Delivery of DNA. *Angew. Chem., Int. Ed.* **2005**, *44*, 4782–4785.
21. Liu, Z.; Winters, M.; Holodniy, M.; Dai, H. siRNA Delivery into Human T Cells and Primary Cells with Carbon-Nanotube Transporters. *Angew. Chem., Int. Ed.* **2007**, *46*, 2023–2027.
22. Yang, R.; Yang, X.; Zhang, Z.; Zhang, Y.; Wang, S.; Cai, Z.; Jia, Y.; Ma, Y.; Zheng, C.; Lu, Y.; Roden, R.; Chen, Y. Single-Walled Carbon Nanotubes-Mediated *in Vivo* and *in Vitro* Delivery of siRNA into Antigen-Presenting Cells. *Gene Ther.* **2006**, *13*, 1714–1723.
23. Schipper, M.; Ratchford, N.; Davis, C.; Kam, N. W. S.; Chu, P.; Liu, Z.; Sun, X.; Dai, H.; Gambhir, S. A Pilot Toxicology Study of Single-Walled Carbon Nanotubes in a Small Sample of Mice. *Nat. Nanotechnol.* **2008**, *3*, 216–221.
24. Singh, R.; Pantarotto, D.; Lacerda, L.; Pastorin, G.; Klumpp, C.; Prato, M.; Bianco, A.; Kostarelos, K. Tissue Biodistribution and Blood Clearance Rates of Intravenously Administered Carbon Nanotube Radiotracers. *Proc. Nat. Acad. Sci. U.S.A.* **2006**, *103*, 3357–3362.
25. Feazell, R.; Ratchford, N.; Dai, H.; Lippard, S. Soluble Single-Walled Carbon Nanotubes as Longboat Delivery Systems for Platinum(IV) Anticancer Drug Design. *J. Am. Chem. Soc.* **2007**, *129*, 8438–8439.
26. Ajima, K.; Yudasaka, M.; Murakami, T.; Maigne, A.; Shiba, K.; Iijima, S. Carbon Nanohorns as Anticancer Drug Carriers. *Mol. Pharm.* **2005**, *2*, 475–480.
27. Wu, W.; Wieckowski, S.; Pastorin, G.; Benincasa, M.; Klumpp, C.; Briand, J.; Gennaro, R.; Prato, M.; Bianco, A. Targeted Delivery of Amphotericin b to Cells by using Functionalized Carbon Nanotubes. *Angew. Chem., Int. Ed.* **2005**, *44*, 6358–6362.
28. Dhar, S.; Liu, Z.; Thomale, J.; Dai, H.; Lippard, S. Targeted Single-Wall Carbon Nanotube-Mediated Pt(IV) Prodrug Delivery Using Folate as a Homing Device. *J. Am. Chem. Soc.* **2008**, *130*, 11467–11476.
29. Liu, Z.; Cai, W.; He, L.; Nakayama, N.; Chen, K.; Sun, X.; Chen, X.; Dai, H. *In Vivo* Biodistribution and Highly Efficient Tumor Targeting of Carbon Nanotubes in Mice. *Nat. Nanotechnol.* **2007**, *2*, 47–52.
30. McDevitt, M.; Chattopadhyay, D.; Kappel, B.; Jaggi, J.; Schiffman, S.; Antczak, C.; Njardarson, J.; Brentjens, R.; Scheinberg, D. Tumor Targeting with Antibody-Functionalized, Radiolabeled Carbon Nanotubes. *J. Nucl. Med.* **2007**, *48*, 1180–1189.
31. Liu, Z.; Chen, K.; Davis, C.; Sherlock, S.; Cao, Q.; Chen, X.; Dai, H. Drug Delivery with Carbon Nanotubes for *in Vivo* Cancer Treatment. *Cancer Res.* **2008**, *68*, 6652–6660.
32. Go, R.; Adjei, A. Review of the Comparative Pharmacology and Clinical Activity of Cisplatin and Carboplatin. *J. Clin. Oncol.* **1999**, *17*, 409–422.
33. Kelland, L. The Resurgence of Platinum-Based Cancer Chemotherapy. *Nat. Rev.* **2007**, *7*, 573–584.
34. Cohen, J. Role of Epidermal Growth Factor Receptor Pathway−Targeted Therapy in Patients with Recurrent and/or Metastatic Squamous Cell Carcinoma of the Head and Neck. *Clin. Oncol.* **2006**, *24*, 2659–2665.
35. Jimeno, A.; Viqueira, B.; Amador, M.; Oppenheimer, D.; Bouraoud, N.; Kulesza, P.; Sebastiani, V.; Maitra, A.; Hidalgo, M. Epidermal Growth Factor Receptor Dynamics Influences Response to Epidermal Growth Factor Receptor Targeted Agents. *Cancer Res.* **2005**, *65*, 3003–3010.
36. Kalyankrishna, S.; Grandis, J. Epidermal Growth Factor Receptor Biology in Head and Neck Cancer. *J Clin. Oncol.* **2006**, *24*, 2666–2672.
37. Zerda, A.; Gambhir, S. Keeping Tabs on Nanocarriers. *Nat. Nanotechnol.* **2007**, *2*, 745–746.
38. Tauro, J. R.; Gemeinhart, R. A. Matrix Metalloprotease Triggered Delivery of Cancer Chemotherapeutics from Hydrogel Matrixes. *Bioconjugate Chem.* **2005**, *16*, 1133–1139.
39. Keskar, V.; Mohanty, P.; Gemeinhart, E.; Gemeinhart, R. Development of a Local System for Treatment of Cervical Cancer. *J. Controlled Release* **2006**, *115*, 280–288.
40. Sriuranpong, V.; Park, J.; Amornphimoltham, P.; Patel, V.; Nelkin, B.; Gutkind, S. Epidermal Growth Factor Receptor-independent Constitutive Activation of Stat3 in Head and Neck Squamous Cell Carcinoma is Mediated by the Autocrine/Paracrine Stimulation of the Interleukin 6/gp130 Cytokine System. *Cancer Res.* **2003**, *63*, 2948–2956.
41. Basile, J. R.; Castilho, R. M.; Williams, V. P.; Gutkind, J. S. Semaphorin 4D Provides a Link between Axon Guidance Processes and Tumor-induced Angiogenesis. *Proc. Natl. Acad. Sci. U.S.A.* **2006**, *103*, 9017–9022.
42. Nozawa, H.; Takushi, T.; Takeshi, O.; Masaki, S.; Sadayuki, H.; Kazuma, M; Yasunori, S. Small interfering RNA Targeting Epidermal Growth Factor Receptor Enhances Chemosensitivity to Cisplatin, 5-Fluorouracil, and Docetaxel in Head and Neck Squamous Cell Carcinoma. *Cancer Sci.* **2006**, *97*, 1115–1124.
43. Welsher, K.; Liu, Z.; Daranciang, D.; Dai, H. Selective Probing and Imaging of Cells with Single Walled Carbon Nanotubes as Near-Infrared Fluorescent Molecules. *Nano Lett.* **2008**, *8*, 586–590.

44. Porter, A.; Gass, M.; Muller, K.; Skepper, J.; Midgley, P.; Welland, M. Direct Imaging of Single-Walled Carbon Nanotubes in Cells. *Nat. Nanotechnol.* **2007**, *2*, 713–717.
45. Amornphimoltham, P.; Patel, V.; Sodhi, A.; Nikitakis, N.; Sauk, J.; Sausville, E.; Molinolo1, A.; Gutkind, S. Mammalian Target of Rapamycin, a Molecular Target in Squamous Cell Carcinomas of the Head and Neck. *Cancer Res.* **2005**, *65*, 9953–9961.
46. Sayes, C.; Liang, F.; Hudson, J.; Mendez, J.; Guo, W.; Beach, J.; Moore, V.; Doyle, C.; West, J.; Billups, W.; Ausmanb, K.; Colvin, V. Functionalization Density Dependence of Single-Walled Carbon Nanotubes Cytotoxicity *in Vitro*. *Toxicol. Lett.* **2006**, *161*, 135–142.
47. Gao, L.; Nie, L.; Wang, T.; Qin, Y.; Guo, Z.; Yang, D.; Yan, X. Carbon Nanotube Delivery of the GFP Gene into Mammalian Cells. *ChemBioChem* **2006**, *7*, 239–242.
48. Liu, Z.; Davis, C.; Cai, W.; He, L.; Chen, X.; Dai, H. Circulation and Long-Term Fate of Functionalized, Biocompatible Single-Walled Carbon Nanotubes in Mice Probed by Raman Spectroscopy. *Proc. Nat. Acad. Sci. U.S.A.* **2007**, *105*, 1410–1415.
49. Ye, H.; Jin, L.; Hu, R.; Yi, Z.; Li, J.; Wu, Y.; Xi, X.; Wu, Z. Poly(g,L-glutamic acid)−Cisplatin Conjugate Effectively Inhibits Human Breast Tumor Xenografted in Nude Mice. *Biomaterials* **2006**, *27*, 5958–5965.
50. Kostarelos, K. The Long and Short of Carbon Nanotube Toxicity. *Nat. Biotechnol.* **2008**, *26*, 774–776.
51. Liu, Z.; Cai, W.; He, L.; Nakayama, N.; Chen, K.; Sun, X; Chen, X.; Dai, H. In Vivo Biodistribution and Highly Efficient Tumour Targeting of Carbon Nanotubes in Mice. *Nat. Nanotechnol.* **2007**, *2*, 47–52.
52. Cherukuri, P.; Bachilo, S. M.; Litovsky, S. H.; Weisman, R. B. Near-Infrared Fluorescence Microscopy of Single-Walled Carbon Nanotubes in Phagocytic Cells. *J. Am. Chem. Soc.* **2004**, *126*, 15638–15639.
53. Sayes, C. M.; Feng Liang, F.; Hudson, J. L.; Mendeza, J.; Guo, W.; Beach, J. M.; Moore, V. C.; Doyle, C. D.; West, J. L.; Billups, W. E.; Ausman, K. D.; Colvin, V. L. Functionalization Density Dependence of Single-Walled Carbon Nanotube Cytotoxicity *in Vitro*. *Toxicol. Lett.* **2006**, *161*, 135–142.
54. Dumortier, H.; Lacotte, S.; Pastorin, G.; Marega, R.; Wu, W.; Bonifazi, D.; Briand, J.-P.; Prato, M.; Muller, S.; Bianco, A. Functionalized Carbon Nanotubes Are Noncytotoxic and Preserve the Functionality of Primary Immune Cells. *Nano Lett.* **2006**, *6*, 1522–1528.
55. Lison, D.; Muller, J. Lung and Systemic Responses to Carbon Nanotubes (CNT) in Mice. *Toxicol. Sci.* **2008**, *101*, 179–180.
56. Varela, M.; Lupini, A.; Benthem, K.; Borisevich, A.; Chisholm, M.; Shibata, N.; Abe, E.; Pennycook, S. Materials Characterization in the Aberration-Corrected Scanning Transmission Electron Microscope. *Ann. Rev. Mater. Res* **2005**, *35*, 539–569.